Optical Engineering

OpticalEngineering.SPIEDigitalLibrary.org

Flexible method for improved transmitter parameter calibration in accurate large-scale positioning system

Qing Liu
Huashuai Ren
Kun Jia
Xiao Pan
Jie Zhang
Haolin Liu

SPIE.

Qing Liu, Huashuai Ren, Kun Jia, Xiao Pan, Jie Zhang, Haolin Liu, "Flexible method for improved transmitter parameter calibration in accurate large-scale positioning system," *Opt. Eng.* **58**(6), 064105 (2019), doi: 10.1117/1.OE.58.6.064105.

Flexible method for improved transmitter parameter calibration in accurate large-scale positioning system

Qing Liu,[a] Huashuai Ren,[a] Kun Jia,[b,*] Xiao Pan,[b] Jie Zhang,[a] and Haolin Liu[a]
[a]Xi'an University of Technology, Engineering Training Center, Xi'an, China
[b]Xi'an Aerocomm Measurement and Control Technology Co., Ltd., Xi'an, China

Abstract. An accurate large-scale positioning system is a three-dimensional workspace measuring and positioning the laser scanning-based system that is widely used in smart manufacturing and assembly applications. The system includes laser transmitters that are typically calibrated using one of two methods: a high-precision rotary table-dependent method or a three-dimensional (3-D) coordinate control network-dependent method. However, these methods are error-prone and inefficient. We propose a flexible calibration method that is based on the transmitter geometry and employs the characteristic angles of the transmitter as calibration targets that do not change with transmitter location or orientation. The proposed method also utilizes a calibration algorithm that is based on a highly precise 3-D coordinate control network and includes an optimization algorithm and an estimation algorithm to produce initial values. The results of Monte Carlo simulations indicate that the proposed method enables the characteristic angles to maintain accuracy within 3 arc sec. Furthermore, the results of verification experiments show that the proposed method decreases the deviation of each control point and the root-mean-square error to 0.075 and 0.052 mm, respectively.
[DOI: 10.1117/1.OE.58.6.064105]

Keywords: accurate large-scale positioning system; parameter calibration; three-dimensional coordinate control network; laser theodolite; characteristic angle.

Paper 190287 received Mar. 1, 2019; accepted for publication May 22, 2019; published online Jun. 20, 2019.

1 Introduction

Large-scale dimensional metrology is widely used in many industrial applications to acquire real-time information during product assembly processes to automatically compensate for assembly tolerances.[1–4] One of the most popular types of metrology systems is the accurate large-scale positioning system (ALPS), which is a distributed contact measurement and positioning instrument that relies on the intersection of rotating laser planes from multiple base stations and incorporates two or more independent laser transmitters, a control center, and a set of wireless sensors.[5–7] The primary advantage of this system is scalability in that users can have as many transmitters and sensors as required by the measurement environment. Compared with traditional technologies, such as laser trackers and theodolites, an ALPS has several advantages, such as large measurement range, multitask parallel measurement, and high degree of automation.

The architecture of an ALPS can be explained by first considering the function of an individual laser theodolite that consists of a transmitter and sensor and constitutes an entire measurement and positioning network. The transmitter covers the area in its vicinity with two rotating fanned laser beams and a strobe. The sensor is placed on the surface of the workpiece and can detect the pulse of light from the strobe and both fanned laser beams. Assuming that the transmitter parameters are known, the relative angles of the lasers can be obtained from the timing differences between the pulses of light that reach the sensor (as explained in Sec. 2 below). Then, the position of the sensor can be calculated by triangulation based on the angle measurements from multiple transmitters. As accurate angle measurement is essential, it is critical that every transmitter is calibrated to ensure that errors do not substantially affect the measurement results.

In general, one of two methods is commonly used for parametric calibration of the transmitter(s). The first determines the geometric parameters using a high-precision rotary table,[8,9] while the other establishes a high-precision three-dimensional (3-D) coordinate control network based on certain constraints.[10] Then, the parameters in both methods are calculated via iterative optimization algorithms. The rotary table-based method requires the transmitter to be mounted coaxially onto the table to ensure the validity of the calibration results; however, this complicates the calibration procedure and can result in artificial errors. To overcome this limitation, Zhao et al.[10] employed a 3-D coordinate control network constructed via a laser tracker to calibrate the parameters of the transmitter and achieved significantly higher accuracy. However, a problem with this revised approach is that the coefficients of the laser-plane equations are considered to be the final calibration results even though these coefficients vary with the location and/or orientation of the transmitter. Thus, to accommodate this variation, the calibration procedure must be repeated before each field measurement, which is time-consuming.

In this paper, we propose a practical calibration method that is based on the intrinsic geometric characteristics of the transmitter, namely the constant characteristic angles. There are two steps in the proposed method. The first is to establish a precise 3-D coordinate control network to obtain the coordinates of all control points via a high-precision 3-D coordinate measuring machine (CMM). The second is to calibrate the characteristic angles based on the constraints of the 3-D control network. This approach has many advantages. The

*Address all correspondence to Kun Jia, E-mail: kunjia0131@163.com

0091-3286/2019/$25.00 © 2019 SPIE

first is that the characteristic angles are constant and do not vary as the location and/or orientation of the transmitters change. Thus, once a transmitter has been calibrated, the corresponding parameters can be reused as needed without requiring recalibration. This reduces the overall calibration time compared to conventional methods and improves the measurement efficiency. The proposed method has been validated experimentally and found to be effective.

The remainder of this paper is organized as follows. Section 2 provides an introduction to the positioning principle of the ALPS and also details a mathematical model of a single laser theodolite and another of the ALPS. A summary of the calibration procedure is presented in Sec. 3, including definitions of the characteristic angles of the transmitter, the optimization model, and the method of estimating the initial iteration values. The experimental results are detailed in Sec. 4, while the conclusions that can be drawn from this study are provided in Sec. 5.

2 Positioning Principle of the Accurate Large-Scale Positioning System

A typical ALPS consists of two or more laser transmitters, a control center, and multiple wireless sensors. Each transmitter operates as a reference point that continually generates three signals, namely, an infrared LED strobe and two rotating fanned laser planes that sweep past the sensor at different moments in time. The geometric structure of the transmitter is shown in Fig. 1. As soon as incident optical signals are detected by the sensor, they are converted into timing signals by a photo detector. Next, the timing intervals are converted into angles based on the speed of rotation of the transmitter. Then, the characteristic angles can be used to estimate the location of a line between the transmitter and the geometric center of the sensor. Based on the locations and orientations of multiple transmitters, the intersection point of the lines connecting the transmitters with the sensor can be determined via the least squares method. This intersection point corresponds to the 3-D position of the sensor.

2.1 *Mathematical Model of a Single Laser Theodolite*

Suppose O-XYZ represents the local coordinate frame of the transmitter during the measurement process and the Y-axis is aligned with the rotational axis of the transmitter. When the sensor detects a pulse of light from the infrared LED strobe, this is referred to as the initial moment. The position of the laser planes at that same moment is called the initial position. Then, in O-XYZ, the initial position of the laser planes can be represented as

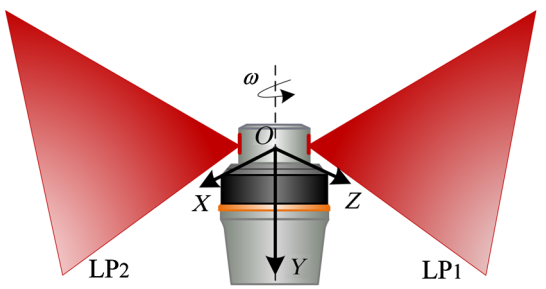

Fig. 1 Geometric model of a transmitter.

$$N_1 \cdot (P - T) = 0 \quad N_2 \cdot (P - T) = 0, \tag{1}$$

where N_1 and N_2 are the vectors normal to laser planes LP_1 and LP_2, respectively, and can be estimated from the characteristic angles of the transmitter, P is an unknown point, and T is the origin of plane O-XYZ.

The transmitter in this scenario is rotating. When the laser planes return to their initial positions, the pulse generated by the infrared LED strobe at that point is defined as being generated at the initial moment. As shown in Fig. 2, the initial moment is denoted as t_0. Planes LP_1 and LP_2, respectively, sweep through point P at t_1 and t_2. Consider LP_1 as an example. The normal vector to plane LP_1 at t_1 is, therefore, given as

$$N_{1\theta} = R_1 N_1 = \begin{bmatrix} \cos\theta_1 & 0 & -\sin\theta_1 \\ 0 & 1 & 0 \\ \sin\theta_1 & 0 & \cos\theta_1 \end{bmatrix} N_1, \tag{2}$$

$$\theta_1 = \omega(t_1 - t_0), \tag{3}$$

where R_1 is the rotational matrix of plane LP_1 about the Y-axis from the initial time t_0 to time t_1, ω is the rotational speed of the spinning head in each transmitter, and θ_1 is as defined as shown in Fig. 2.

At t_1, the plane LP_1 in O-XYZ can be represented as

$$(R_1 N_1) \cdot (P - T) = 0. \tag{4}$$

Similarly, at t_2, plane LP_2 in O-XYZ can be written as

$$(R_2 N_2) \cdot (P - T) = 0. \tag{5}$$

Suppose the time delays of planes LP_1 and LP_2 sweeping past point P can be ignored. The intersecting line of planes LP_1 and LP_2 passing through P in O-XYZ can therefore be written as

$$\begin{cases} (R_1 N_1) \cdot (P - T) = 0 \\ (R_2 N_2) \cdot (P - T) = 0 \end{cases}. \tag{6}$$

2.2 *Mathematical Model of the Accurate Large-Scale Positioning System*

As mentioned above, for a single transmitter, it is possible to determine the line joining the transmitter with point P. This means that for all transmitters, many lines connect different transmitters with point P. The line connected to the n'th transmitter can be represented as

$$\begin{cases} (R_{1n} N_{1n}) \cdot (P - T_n) = 0 \\ (R_{2n} N_{2n}) \cdot (P - T_n) = 0 \end{cases}. \tag{7}$$

In ALPS, the world coordinate frame is defined as O_w-$X_w Y_w Z_w$ and the line of the n'th transmitter through point P in O_w-$X_w Y_w Z_w$ can be written as

$$\begin{cases} (R_n R_{1n} N_{1n}) \cdot (P - T_n) = 0 \\ (R_n R_{2n} N_{2n}) \cdot (P - T_n) = 0 \end{cases}, \tag{8}$$

where R_n is the rotational matrix of the n'th transmitter from O_n-$X_n Y_n Z_n$ to O_w-$X_w Y_w Z_w$ and T_n is the coordinate of the origin of O_n-$X_n Y_n Z_n$ in O_w-$X_w Y_w Z_w$.

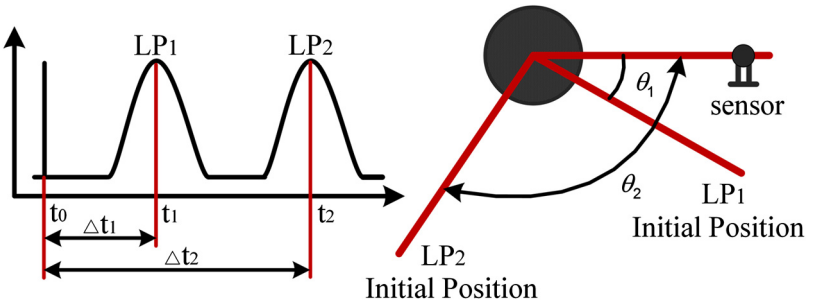

Fig. 2 Relationship between a typical pulse sequence and the rotational angles during a single rotation.

Thus, when the number of transmitters equals or exceeds two, point P in O_w-$X_wY_wZ_w$ can be determined by solving the following nonlinear equations:

$$\begin{cases} (R_1R_{11}N_{11})\cdot(P-T_1)=0 \\ (R_1R_{21}N_{21})\cdot(P-T_1)=0 \\ (R_2R_{12}N_{12})\cdot(P-T_2)=0 \\ (R_2R_{22}N_{22})\cdot(P-T_2)=0 \\ \vdots \\ (R_nR_{1n}N_{1n})\cdot(P-T_n)=0 \\ (R_nR_{2n}N_{2n})\cdot(P-T_n)=0 \end{cases}, \tag{9}$$

where n is the number of transmitters, R_{1n} and R_{2n} are the rotational matrices of the laser planes about the Y-axis, N_{1n} and N_{2n} are the vectors normal to the laser planes in the initial position, R_n is the rotational matrix from O_n-$X_nY_nZ_n$ to O_w-$X_wY_wZ_w$, T_n is the coordinate of the origin of O_n-$X_nY_nZ_n$ in O_w-$X_wY_wZ_w$, and P is the coordinate of the measured point in O_w-$X_wY_wZ_w$.

Once the characteristic angles of the transmitter have been calibrated, it then becomes possible to determine N_{1n} and N_{2n}. The values of R_n and T_n can be optimized using the spherical constraints method described by Zhao et al.[11] The coordinates of the measured point P in O_w-$X_wY_wZ_w$ can then be estimated using the least squares method.

3 Calibration of the Characteristic Angles

As stated above, it is essential that the characteristic angles be calibrated before the ALPS is employed to estimate N_{1n} and N_{2n}. The method of calibration is introduced in this section.

3.1 *Characteristic Angles of a Transmitter*

The characteristic angles are defined as shown in Fig. 3. In the figure, the two fanned laser planes that emit from the rotating head of each transmitter are nominally tilted with respect to the axis of rotation at $\varphi_1 \approx 30$ deg and $\varphi_2 \approx -30$ deg, where φ_{off} describes the angular separation between the two laser modules located in the rotating head of each transmitter and is nominally $\varphi_{\text{off}} \approx 90$ deg. These three parameters are referred to as the characteristic angles of the transmitter that are used to calculate the unknown parameters N_{1n} and N_{2n} in the measurement phase.

3.2 *Optimization Model of the Characteristic Angles*

There are two phases in the optimization procedure: data collection and data processing. In the data collection phase, a sensor similar to the one depicted in Fig. 4 is affixed on a 3-D CMM, while the transmitter is located some distance away. The location of the control point is measured continuously by the CMM, while the sensor is moved over a known distance on the guide rails of the CMM. The measured control points are then processed during the data-processing phase. In this stage, the coordinate frame of the CMM is

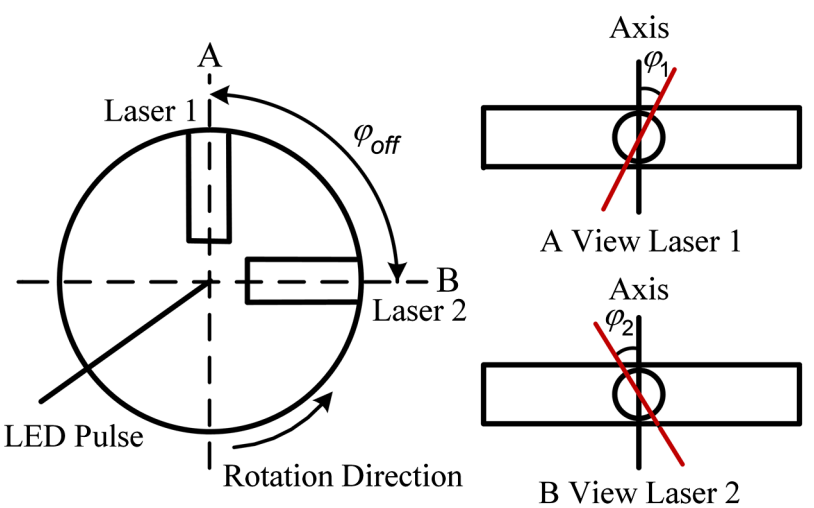

Fig. 3 Characteristic angles of a transmitter.

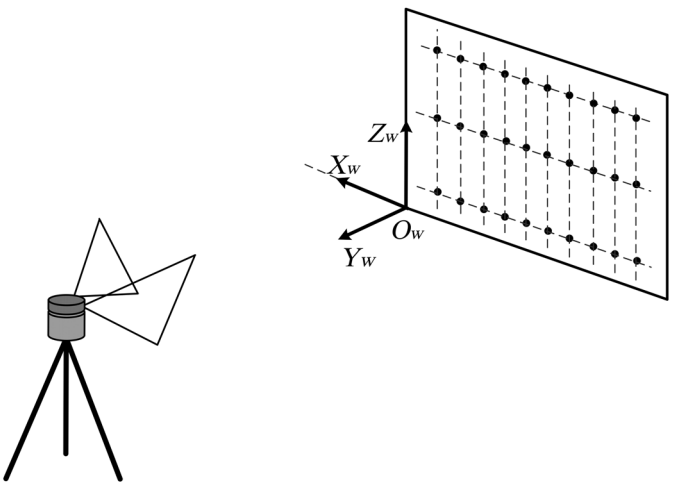

Fig. 4 Characteristic angle calibration procedure.

defined as the global coordinate reference system and is denoted as O_w-$X_wY_wZ_w$. As per the measurement principle, as each observation is made, the line from the transmitter in O_w-$X_wY_wZ_w$ through control point P can be represented as

$$\begin{cases} (RR_1N_1)\cdot(P_n-T)=0 \\ (RR_2N_2)\cdot(P_n-T)=0 \end{cases}, \tag{10}$$

where n is the number of control points, R_1 and R_2 are the rotational matrixes of the two laser planes with respect to the rotational axis and are a function of time Δt_1 and Δt_2, N_1 and N_2 are the normal vectors to the laser planes at the initial position, R is the rotational matrix from the local coordinate frame of transmitter O-XYZ to O_w-$X_wY_wZ_w$, T is the coordinate of the origin of O-XYZ in O_w-$X_wY_wZ_w$, and P_n is the coordinate of the control point in O_w-$X_wY_wZ_w$.

To obtain a unique solution, the values of the parameters B_1 and B_2 in N_1 and N_2 are set to 1. Then, the normal vectors to the laser planes at the initial position and in the rotational matrix can be written as follows:

$$N_1=(A_1 \quad 1 \quad C_1)^T, \qquad N_2=(A_2 \quad 1 \quad C_2)^T,$$

$$\begin{aligned} R&=(r_x,r_y,r_z)=R_xR_yR_z \\ &=\begin{bmatrix} 1 & 0 & 0 \\ 0 & \cos r_x & -\sin r_x \\ 0 & \sin r_x & \cos r_x \end{bmatrix}\begin{bmatrix} \cos r_y & 0 & \sin r_y \\ 0 & 1 & 0 \\ -\sin r_y & 0 & \cos r_y \end{bmatrix} \\ &\times\begin{bmatrix} \cos r_z & -\sin r_z & 0 \\ \sin r_z & \cos r_z & 0 \\ 0 & 0 & 1 \end{bmatrix}. \end{aligned} \tag{11}$$

There are three unknown parameters in T, which are denoted as t_x, t_y, and t_z. Hence, the transmitter calibration process includes 10 unknown parameters: A_1, B_1, A_2, B_2, r_x, r_y, r_z, t_x, t_y, and t_z. Obtaining solutions for these parameters requires n ($n \geq 5$) control points in the optimization. The resulting system of equations is as follows:

$$\begin{cases} (RR_{11}N_1)\cdot(P_1-T)=0 \\ (RR_{21}N_2)\cdot(P_1-T)=0 \\ (RR_{12}N_1)\cdot(P_2-T)=0 \\ (RR_{22}N_2)\cdot(P_2-T)=0 \\ \vdots \\ (RR_{1n}N_1)\cdot(P_n-T)=0 \\ (RR_{2n}N_2)\cdot(P_n-T)=0 \end{cases}. \tag{12}$$

Based on above system of equations and the given initial values of parameters A_1^0, B_1^0, A_2^0, B_2^0, r_x^0, r_y^0, r_y^0, t_z^0, t_y^0, and t_z^0, the optimal solution can be obtained via the Levenberg–Marquardt[12,13] iterative algorithm. The objective function is then defined as

$$J=\sum_{i=1}^{n}\{[(RR_{1i}N_1)\cdot(P_i-T)]^2+[(RR_{2i}N_2)\cdot(P_i-T)]^2\}. \tag{13}$$

Of the 10 parameters, A_1, B_1, A_2, and B_2 are the most important as they can be employed to directly compute the characteristic angles φ_1, φ_2, and φ_{off}. As shown in Fig. 5, once a value for N_1 has been determined, plane LP_1 in the initial position can be represented in O-XYZ as

$$A_1x+y+C_1z=0. \tag{14}$$

The line of intersection between plane LP_1 and plane XOZ is denoted as L_1 and has the slope

$$k_1=-\frac{A_1}{C_1}. \tag{15}$$

In XOZ, line L_3 is perpendicular to L_1 and direction vector N_3 is normal to the plane LP_3. Thus, their slopes must satisfy the following relationship:

$$k_1k_3=-1. \tag{16}$$

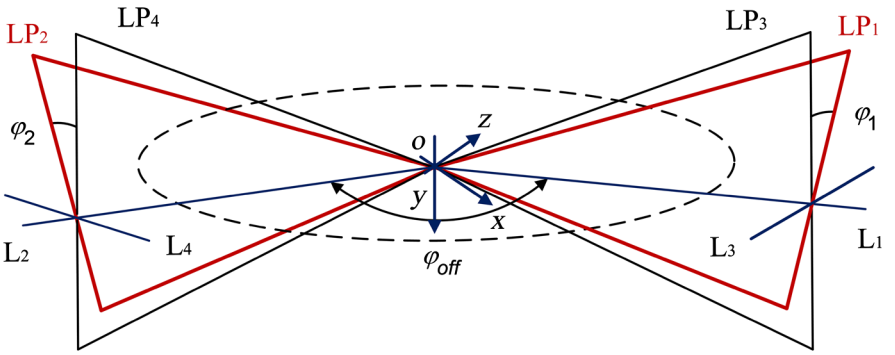

Fig. 5 Calculation of the characteristic angles.

In O-XYZ, N_3 can then be represented as

$$N_3 = \begin{pmatrix} 1 & \frac{C_1}{A_1} & 0 \end{pmatrix}^T. \tag{17}$$

The angle between planes LP_1 and LP_3 is the characteristic angle φ_1, which is simply the angle between vectors N_1 and N_3. Therefore, φ_1 can be represented as

$$\cos\varphi_1 = \frac{A_1 + \frac{C_1^2}{A_1}}{\sqrt{A_1^2 + C_1^2}\sqrt{1 + \frac{C_1^2}{A_1^2}}}. \tag{18}$$

Similarly, the characteristic angle φ_2 can be represented as

$$\cos\varphi_2 = \frac{A_2 + \frac{C_2^2}{A_2}}{\sqrt{A_2^2 + C_2^2}\sqrt{1 + \frac{C_2^2}{A_2^2}}}. \tag{19}$$

The slope of L_2, which is the line of intersection between plane LP_2 and plane XOZ, is given as

$$k_2 = -\frac{A_2}{C_2}. \tag{20}$$

The characteristic angle φ_{off}, which is the angle between lines L_1 and L_2 in O-XYZ, can be represented as

$$\cos\varphi_{\text{off}} = \frac{1 + \frac{A_1 A_2}{C_1 C_2}}{\sqrt{1 + \frac{A_1^2}{C_1^2}}\sqrt{1 + \frac{A_2^2}{C_2^2}}}. \tag{21}$$

3.3 *Estimating the Initial Iteration Values*

As mentioned above, an essential condition to solve the optimization problem described in Sec. 3.2 is the ability to obtain a suitable initial iteration value for the equations. Initial iteration values A_1^0, B_1^0, A_2^0, and B_2^0 are the elements of the initial normal vectors N_{1n} and N_{2n} that can be derived directly from the characteristic angles φ_1, φ_2, and φ_{off}. Computing N_{1n} begins with a vertical plane at $x = 0$, which is a plane in the $Y - Z$ axis of which the normal vector is denoted as $(1,0,0)^T$. When this vertical plane is rotated around the Z-axis by an angle φ_1, the result is as shown in Fig. 6. This new plane represents the first fanned laser inserted into the head of the transmitter. A vector normal to the new plane can be represented as

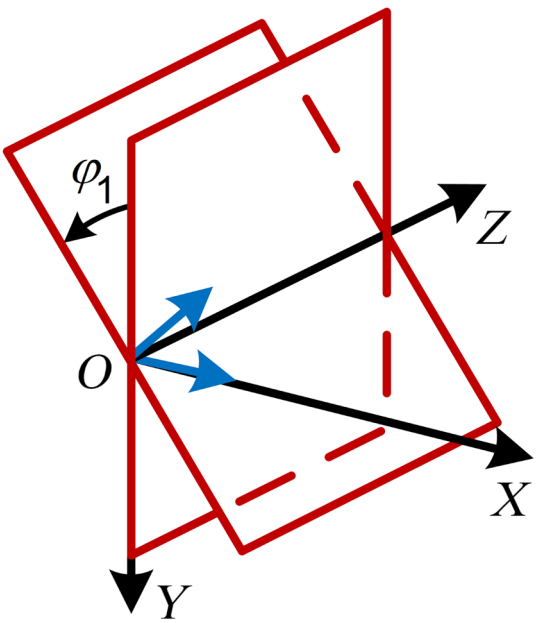

Fig. 6 Fanned beam rotated about the Z-axis.

$$\begin{bmatrix} \cos\varphi_1 & \sin\varphi_1 & 0 \\ -\sin\varphi_1 & \cos\varphi_1 & 0 \\ 0 & 0 & 1 \end{bmatrix} \begin{bmatrix} 1 \\ 0 \\ 0 \end{bmatrix} = \begin{bmatrix} \cos\varphi_1 \\ -\sin\varphi_1 \\ 0 \end{bmatrix}. \tag{22}$$

Suppose we then rotate the new plane about the Y-axis by an angle θ_1 in intervals of time Δt_1, until it is opposite to the initial position, then, N_{1n}, which is the normal vector to plane LP_1 in the initial position, can be represented as

$$N_{1n} = \begin{bmatrix} \cos\theta_1 & 0 & \sin\theta_1 \\ 0 & 1 & 0 \\ -\sin\theta_1 & 0 & \cos\theta_1 \end{bmatrix} \begin{bmatrix} \cos\varphi_1 \\ -\sin\varphi_1 \\ 0 \end{bmatrix}. \tag{23}$$

Similarly, N_{2n}, which is the normal vector to plane LP_2 in the initial position, can be represented as

$$N_{2n} = \begin{bmatrix} \cos\theta_1 & 0 & \sin\theta_1 \\ 0 & 1 & 0 \\ -\sin\theta_1 & 0 & \cos\theta_1 \end{bmatrix} \begin{bmatrix} -\cos\varphi_{\text{off}}\cos\varphi_2 \\ -\sin\varphi_2 \\ \sin\varphi_{\text{off}}\cos\varphi_2 \end{bmatrix}. \tag{24}$$

As per the geometry of the transmitter, the initial values of the characteristic angles φ_1, φ_2, and φ_{off} are chosen to be 30 deg, −30 deg, and 90 deg, respectively. The initial iteration values A_1^0, B_1^0, A_2^0, and B_2^0 can then be estimated via Eqs. (23) and (24).

The problem of estimating the initial values r_x^0, r_y^0, r_y^0, t_z^0, t_y^0, and t_z^0 can be viewed as a perspective-n-point[14,15] (PnP) problem, which is the problem of estimating the pose of a calibrated camera based on a given set of n 3-D points in the real world and their corresponding two-dimensional projections in the image. The given image points are derived based on the time Δt_1 and Δt_2 and the position of each control point in O_w-$X_wY_wZ_w$. The initial iteration values r_x^0, r_y^0, r_y^0, t_z^0, t_y^0, and t_z^0 are obtained by solving the PnP problem.

4 Experimental Results

The validity of the proposed method was evaluated as follows. The characteristic angle calibration method was tested via Monte Carlo simulation, which is a technique used to study how a model responds to randomly generated inputs. Based on the uncertainties in the transmitter, sensor, and CMM—such as the angular velocity deviation of the transmitter, the time deviation of the laser signal detected by the sensor, and the control point coordinates deviation measured by the CMM—the uncertainties in the characteristic angles were propagated from the calibration model using Monte Carlo simulation, which showed how the characteristic angles uncertainties were affected by these parameters. Further, the accuracy of the proposed approach was evaluated via an experiment involving an individual transmitter–sensor pair functioning as a laser theodolite. In the experiment, the deviation in the control points was compared to the results of the previous experiment carried out by Zhao et al.[10]

4.1 *Simulation of the Characteristic Angle Calibration Method*

The simulation model was constructed in 3-D computer-aided design (CAD) software and independently verified via MATLAB. The verification procedure involved the creation of multiple control points at the known coordinates in the CAD model. Further, planes with angles φ_1, φ_2, and φ_{off} were created to simulate the laser planes. These planes were rotated about the Y-axis until they were coincident with each control point. This allowed the rotation angles to be measured and used to compute the rotation time via the CAD software. The time values were then input into the MATLAB simulation, including estimation simulation of iterative initial values and optimization simulation of characteristic angles. The characteristic angles obtained by the MATLAB simulation were then compared with the angles of the original planes in the CAD model.

Because of the angular velocity deviation of the transmitter, the time deviation of the laser signal detected by the sensor and the control point coordinates deviation measured by the CMM were input to the simulation as uncertainties; the uncertainties in the characteristic angles were propagated in the proposed Monte Carlo simulation model. The nominal value and uncertainty of each variable in these equations were estimated, as detailed in Table 1. The simulation results are shown in Fig. 7, where it can be seen that the errors in characteristic angles φ_1, φ_2, and φ_{off} were all <3 arc sec when the proposed calibration method was employed. These results confirm the validity of the proposed calibration method for a single transmitter.

Table 1 Variables used in the mathematical model.

Variable	Nominal	Standard uncertainty	Unit	Description
t_0	0	10×10^{-9}	S	Time measurement strobe signal received by sensor
t_1	—	10×10^{-9}	S	Time measurement plane LP_1 signal received by sensor
t_2	—	10×10^{-9}	S	Time measurement plane LP_2 signal received by sensor
t_3	—	10×10^{-9}	S	Time measurement for transmitter to rotate by α
x	—	0.33×10^{-6}	m	X-coordinate of the control point
y	—	0.33×10^{-6}	m	Y-coordinate of the control point
z	—	0.33×10^{-6}	m	Z-coordinate of the control point
α	2π	485×10^{-9}	rad	Angular interval for counting the rotation of the transmitter
ω	314	α/t_3	rad/s	Angular velocity of transmitter
φ_1	—	—	rad	Angle of inclination of plane LP_1
φ_2	—	—	rad	Angle of inclination of plane LP_2
φ_{off}	—	—	rad	Separation angle between two laser modules

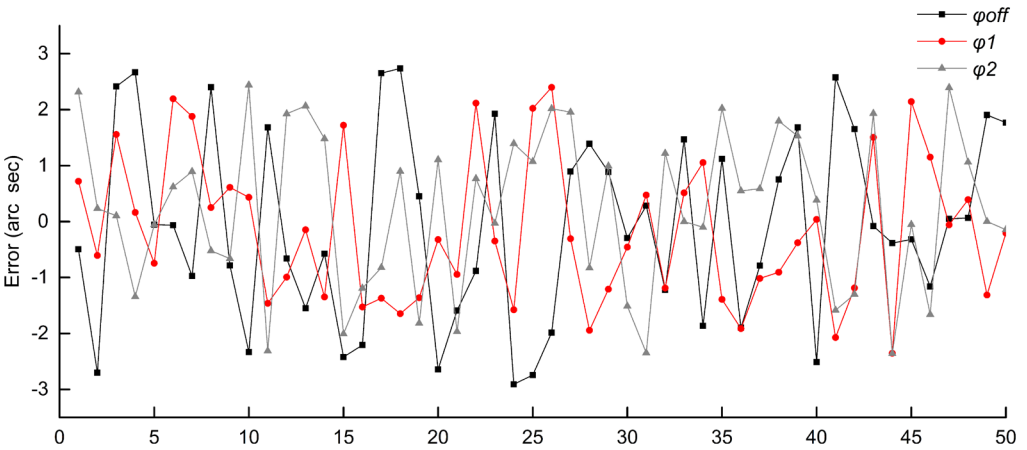

Fig. 7 Errors in the characteristic angles.

4.2 *Accuracy Comparison Experiment*

To validate the proposed method, an experiment was conducted in a 3-D coordinate measurement laboratory to compare the deviation in the distances from each control point to the laser plane with the results of previous transmitter parameter calibration experiments conducted by Zhao et al.[10] The control network comprised 30 points within the measurement range of the 3-D CMM. The measurement accuracy of each point was 0.001 mm. The experimental setup is shown in Fig. 8. One sensor was mounted on the measurement arm of the 3-D CMM and the transmitter was mounted in front of the CMM to ensure that each control point could be detected. Then, the characteristic angles of the transmitter were calibrated via the optimization algorithm described in Sec. 3.2 and the algorithm for estimating the initial iteration values described in Sec. 3.3. Then, the residual errors and root-mean-square error (RMSE) were calculated in order to evaluate the deviation of the points.

Fig. 8 Experimental setup.

In Zhao et al.'s experiment,[10] the control network was established by a laser tracker. Then, transmitter parameter calibration was completed by optimizing the coefficients of the laser-plane equations based on the constraints of the control network. Their experimental results showed that the residual errors in the distance of each control point to the laser plane were <0.1 mm and the RMSE was approximately 0.06 mm.

From the data in Table 2, it can be seen that the residual errors in the distance of each control point to the fanned laser plane are −0.075 to 0.075 mm and the RMSE is 0.052 mm. These results are significantly better than those in the transmitter parameter calibration method based on optimizing the coefficients of the laser-plane equations. Thus, this demonstrates that the proposed calibration method is better able to describe the geometric characteristics of the transmitter and thereby improve the positioning accuracy and efficiency of an ALPS.

5 Conclusions

The use of large-volume measurement and positioning systems has expanded rapidly to accommodate the rising complexity and flexibility of production systems. To satisfy this demand, we propose a modularized large-scale positioning system that we refer to as the ALPS. As a distributed system, ALPS can include multiple transmitters, all of which must be calibrated to ensure positional accuracy during operation. In contrast to conventional approaches, the proposed method employs the characteristic angles of the transmitter as the final calibration targets and then applies a calibration method based on a high-accuracy 3-D coordinate control network. The results of a Monte Carlo simulation show that the accuracy of the characteristic angles once calibrated via the proposed method are maintained within 3 arc sec. The results of a comparison experiment demonstrate that the deviation of each control point after calibration is 0.075 mm and the RMSE is 0.052 mm. These results indicate that the proposed method is feasible and provides good accuracy. Considering

Table 2 Residual errors in the control points (units: millimeter).

Points	Coordinates of control points			Residual error		Points	Coordinates of control points			Residual error	
	x	y	z	d_1	d_2		x	y	Z	d_1	d_2
1	0	0	0	−0.042	0.074	16	250	300	200	0.048	0.018
2	50	0	0	−0.019	−0.066	17	300	300	200	−0.018	0.067
3	100	0	0	−0.063	0.067	18	350	300	200	0.018	−0.022
4	150	0	0	0.021	−0.073	19	400	300	200	0.011	−0.014
5	200	0	0	−0.049	0.028	20	450	300	200	0.005	0.074
6	250	0	0	−0.069	0.043	21	0	600	400	−0.054	0.068
7	300	0	0	0.054	0.005	22	50	600	400	−0.058	0.027
8	350	0	0	−0.023	0.059	23	100	600	400	−0.007	0.074
9	400	0	0	0.024	0.061	24	150	600	400	−0.041	0.041
10	450	0	0	−0.018	0.019	25	200	600	400	0.046	−0.025
11	0	300	200	0.019	−0.055	26	250	600	400	0.074	0.025
12	50	300	200	−0.073	−0.043	27	300	600	400	−0.071	−0.059
13	100	300	200	0.062	−0.048	28	350	600	400	0.005	−0.051
14	150	300	200	0.046	−0.07	29	400	600	400	−0.063	0.027
15	200	300	200	0.057	−0.06	30	450	600	400	0.046	0.004
						RMSE	—	—	—	0.0463	0.0511

the invariance of the characteristic angles of the transmitter, the calibration results can be reused before every field measurement without requiring recalibration, which improves the measurement efficiency.

Acknowledgments

This research was funded by the National Natural Science Foundation of China (61502385) and the Key Research and Development Project of Shaanxi Province (S2018-YF-ZDGY-0583).

References

1. J. E. Muelaner and P. G. Maropoulos, "Large volume metrology technologies for the light controlled factory," *Procedia CIRP* **25**, 169–176 (2014).
2. F. Franceschini et al., "Large-scale dimensional metrology (LSDM): from tapes and theodolites to multi-sensor systems," *Int. J. Precis. Eng. Manuf.* **15**, 1739–1758 (2014).
3. H. Z. Bai, "Optimization for calibration model of workspace measurement positioning system (wMPS) based on distance constraint," *Lasers Eng.* **42**, 113–128 (2019).
4. V. Molebny et al., "Laser radar: historical prospective—from the East to the West," *Opt. Eng.* **56**(3), 031220 (2016).
5. Z. Xiong et al., "Multi-station network layout optimization of workspace measuring and positioning system," in *Proc. Int. Conf. Electr. Eng. and Autom. (EEA2016)*, pp. 110–117 (2017).
6. Z. Liu et al., "A large scale 3D positioning method based on a network of rotating laser automatic theodolites," in *Proc. IEEE Int. Conf. Inf. and Autom.*, Harbin, China, pp. 513–518 (2010).
7. Z. Liu et al., "Mobile large scale 3D coordinate measuring system based on network of rotating laser automatic theodolites," *Proc. SPIE* **7544**, 75446P (2010).
8. J. E. Muelaner et al., "iGPS—an initial assessment of technical and deployment capability," in *3rd Int. Conf. Manuf. Eng.*, pp. 805–810 (2008).
9. J. E. Muelaner et al., "Verification of the indoor GPS system, by comparison with calibrated coordinates and by angular reference," *J. Intell. Manuf.* **23**, 2323–2331 (2012).
10. Z. Zhao et al., "Transmitter parameter calibration of the workspace measurement and positioning system by using precise three-dimensional coordinate control network," *Opt. Eng.* **53**(8), 084108 (2014).
11. Z. Zhao et al., "Optimization for calibration of large-scale optical measurement positioning system by using spherical constraint," *J. Opt. Soc. Am. A* **31**, 1427–1435 (2014).
12. J. J. Moré, "The Levenberg-Marquardt algorithm: implementation and theory," *Lect. Notes Math.* **630**, 105–116 (1978).
13. J. Liu et al., "Algorithm for camera parameter adjustment in multicamera systems," *Opt. Eng.* **54**(10), 104108 (2015).
14. F. Moreno-Noguer et al., "Accurate non-iterative o(n) solution to the PnP problem," in *IEEE 11th Int. Conf. Comput. Vision*, IEEE, pp. 1–8 (2007).
15. V. Lepetit et al., "EPnP: an accurate o(n) solution to the PnP problem," *Int. J. Comput. Vision.* **81**(2), 155–166 (2009).

Qing Liu received his PhD from Xi'an Jiaotong University, China, in 2009. Currently, he is an associate professor at the Engineering Training Center, Xi'an University of Technology. His research interests include laser and photoelectric measurement technology, such as industrial online measurement and large-scale precision metrology.

Huashuai Ren is a master's student at the Engineering Training Center, Xi'an University of Technology. His research interests include laser and photoelectric measurement technology, such as industrial online measurement and large-scale precision metrology.

Kun Jia is the corresponding author of this paper. He received his master's degree in 2013. Currently, he is an engineer at Xi'an

Aerocomm Measurement and Control Technology Co., Ltd. His activities involve laser and photoelectric measurement technology, such as industrial online measurement and large-scale precision metrology.

Xiao Pan received his master's degree in 2013. Currently, he is an engineer at Xi'an Aerocomm Measurement and Control Technology Co., Ltd. His activities involve vision measurement and photoelectric measurement technology.

Jie Zhang is a master's student at the Engineering Training Center, Xi'an University of Technology. His research interests include laser and large-scale precision metrology.

Haolin Liu received his master's degree in 2018. Currently, he is a teaching assistant in the Engineering Training Center, Xi'an University of Technology. His research interests include vision measurement and large-scale precision metrology.